Journal of Applied Physics

Irradiation-enhanced torsional buckling capacity of carbon nanotube bundles

Cite as: J. Appl. Phys. **128**, 195902 (2020); https://doi.org/10.1063/5.0013229
Submitted: 09 May 2020 • Accepted: 30 October 2020 • Published Online: 17 November 2020

Joseph Wallace, Di Chen and Lin Shao

Journal of Applied Physics ARTICLE scitation.org/journal/jap

Irradiation-enhanced torsional buckling capacity of carbon nanotube bundles

Cite as: J. Appl. Phys. **128**, 195902 (2020); doi: 10.1063/5.0013229
Submitted: 9 May 2020 · Accepted: 30 October 2020 ·
Published Online: 17 November 2020

View Online Export Citation CrossMark

Joseph Wallace,[1] Di Chen,[2] and Lin Shao[1,a)]

AFFILIATIONS

[1]Department of Nuclear Engineering, Texas A&M University, College Station, Texas 77843, USA
[2]Texas Center for Superconductivity, University of Houston, Houston, Texas 77204, USA

[a)]**Author to whom correspondence should be addressed:** lshao@tamu.edu

ABSTRACT

Molecular dynamics simulations are used to understand the torsional buckling of pristine and irradiated carbon nanotube (CNT) bundles. Irradiation-induced inter-tube defects are shown to significantly increase the critical buckling torque and critical buckling angle, while slightly increasing the torsional stiffness. In contrast, intra-tube defects are found to degrade the torsional properties. Such competing interactions cause irradiation enhancement to occur in large bundles where significant inter-tube bonding can occur. However, the irradiation enhancement effect becomes weak for very large bundles in which enhanced inter-tube interactions already exist in unirradiated bundles. In pristine CNT bundles of all sizes under torsional loading, CNTs can slip via the weakly interacting van der Waals force, whereas in the irradiated bundles, the inter-tube defects prevent slipping. The study further shows that the formation of one-dimensional carbon chain defects contributes to enhanced friction under slipping.

I. INTRODUCTION

Electron and ion irradiation of carbon nanotubes (CNTs) is a well-known method for tailoring the mechanical properties of CNTs.[1–5] Irradiation of CNT bundles often produces inter-tube defects (cross-links) and intra-tube defects.[1–5] Although such defects can lead to degradation, in some cases, such defects can be used to enhance the mechanical properties of CNTs.[1–5] For example, Kis *et al.* irradiated CNT bundles with an electron beam leading to a 30-fold increase in bending modulus due to the formation of stable inter-tube cross-links.[2] In contrast, the formation of intra-tube defects led to a decrease in strength.

Although many of the proposed novel nanomechanical systems[6–9] and nanocomposites[10,11] depend on the torsional properties of CNT bundles, the irradiation response of such properties has received considerably less attention. Yakobson *et al.* were the first to investigate the response of pristine CNTs to torsional loading using molecular dynamics (MD) simulation.[12] Their study revealed several ways in which CNTs could "buckle" under stress. This buckling phenomenon occurs when the CNT is pushed beyond a critical strain resulting in a release of energy and a switch to a different morphological pattern. In torsional buckling, CNTs are rotated axially until a critical condition is reached at which the walls of CNTs collapse inward, resulting in a flattened CNT morphology. When defects are introduced into the CNT, the torsional response further complicates. Zhang *et al.* studied the effect of various vacancy defect structures on the buckling properties of isolated CNTs.[13] Results revealed that unreconstructed monovacancies, bivacancies, and line defects significantly lowered the critical buckling torque, whereas Stone–Thrower–Wales (STW) defects had only a weak effect.[13] Effects of other imperfection, including bents,[14] impurity capping,[15] and C60 filling,[16] have been investigated. CNT's mechanical property was also found to be sensitive to the surrounding environments, such as water molecules, if CNTs are submerged in water.[17] All these studies show the complexity of buckling phenomena and the rich science behind them.

Mechanical properties of multi-walled CNTs (MWCNTs) are different from single-walled CNTs (SWCNTs) due to inter-wall interactions. Adding interstitials between walls of MWCNTs can increase loading transfer, stiffness, shear resistance, and critical bucking strains.[18–21] The effects of inter-wall bond formation make buckling behaviors of MWCNTs deviated from the classical shell theory.[20] By judiciously introducing defects into MWCNTs, property tuning becomes possible and controllable. Inter-wall defects can be easily introduced through ion and electron irradiation. With electron irradiation, the force loading capacity of MWCNTs was increased by a factor of >10 due to irradiation-induced cross-linking defects.[22]

The present study aims to gain an understanding of ion irradiation effects on CNT bundles of different sizes. Different from SWCNTs and MWCNTs, the torsional response of defective CNT bundles is likely very different from that of isolated CNTs for two reasons: (1) CNT bundles can form cross-linking defects and (2) CNTs in the periphery of a bundle experience a combination of torsional, shear, and tensile deformation. The problem is complicated due to the combined effects from inter-defects, intra-defects, and tube–tube interactions.

II. METHODOLOGY

We investigated the torsional properties of irradiated single-walled carbon nanotube (SWCNTs) bundles of various sizes using MD simulations. The critical buckling torque, critical buckling angle, and torsional stiffness were analyzed as a function of irradiation dose for bundles of different sizes. A torsional strengthening with irradiation was observed for large bundles (strongly in 12 CNTs and slightly in 19 CNTs), whereas a slight torsional weakening was observed in smaller CNT bundles (3 CNTs and 7 CNTs). The atomistic details describing the strengthening mechanism were shown and provided an explanation of why the strengthening would occur in large bundles but not in smaller bundles.

Molecular dynamics simulations were performed using the large-scale atomic/molecular massively parallel simulator (LAMMPS) to integrate Newton's equations of motion via a Verlet integration scheme.[23] All CNTs used in this study were 14×14 chirality with a length of 27.5 nm. The inter-tube spacing was 3.4 Å in accordance with experimentally determined values.[24] A Tersoff potential was used to describe carbon interactions,[25] and the potential was smoothly changed to Zeigler–Biersack–Littmark potential at short ranges.[26] Such a hybrid potential is widely used for modeling irradiation damage in materials due to its ability to accurately describe ballistic collisions.

Irradiations were simulated by introducing 350 eV C atoms from a ring concentric with the bundle axis. During irradiations, the system was under a microcanonical (NVE) ensemble. Between each irradiation, the system was brought back to equilibrium at 300 K using a Langevin thermostat.[27] The ion irradiation was repeated every 2.7 ps, until the desired irradiation level was obtained. The desired levels were the total number of C atoms bombarded, which are 100, 200, 300, and 600, respectively. After irradiation, the potential was switched to the Adaptive Intermolecular Reactive Empirical Bond Order (AIREBO) Potential, which is capable of describing the inter-tube Van der Waals force.[28] The system was then brought to 0.1 K and relaxed for 4 ps. Next, the torsion was applied by a two-step process in which the top and bottom 5 Å were first rotated in opposite directions and then allowed to relax in the vertical direction. The relative rotational speed was 0.017 rad/ps. Between every 0.2°, the top and bottom atoms were also allowed to relax along the bundle axis direction for 0.1 ps. The torque was calculated at each step.

III. RESULTS AND DISCUSSION

Figures 1(a)–1(d) compares the torque vs torsional angle for the 3, 7, 12, and 19 CNT bundles, respectively, at radiation damage levels ranging from 0 to 600° ion bombardments. Each of the pristine bundle curves differs from that of the isolated CNTs studied by Zhang *et al.* in several ways.[13] First, the torque in isolated CNTs increases linearly until the CNT buckles, after which no additional force is required to continue rotating. The pristine CNT bundles demonstrate a similar linear behavior at low torque; however, upon reaching the critical buckling angle, they experience a two-step buckling. As shown in Fig. 1(a), the pristine 3 CNT bundle shows two drops. The first drop occurs at about 38°, and the second drop occurs at about 70°. The pristine 7 CNT bundle [Fig. 1(b)] also shows a similar two-step buckling behavior. The second drop is very weak for the 12 CNT bundle [Fig. 1(c)] and disappears for the 19 CNT bundle [Fig. 1(d)].

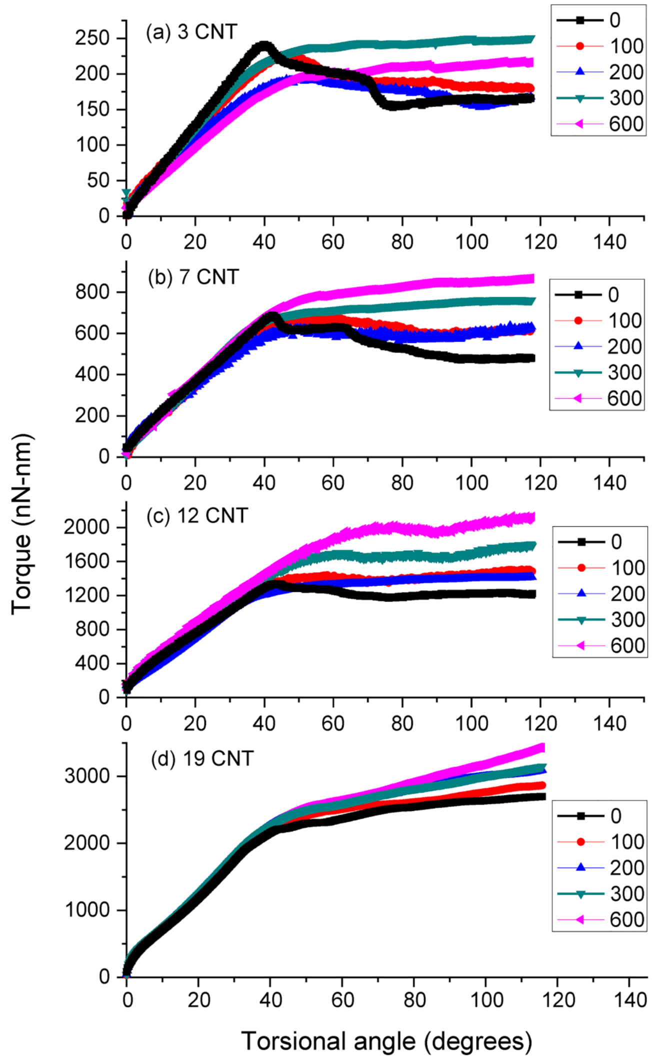

FIG. 1. Torque as a function of torsional angle for (a) 3 CNT, (b) 7 CNT, (c) 12 CNT, and (d) 19 CNT bundles irradiated by 350 eV C atoms to different bombardment numbers.

Figures 2(a) and 2(b) show the side view and cross-sectional view of 3 CNT bundles at different torsional angles. The color represents potential energy. Note the angles of 36° and 42° are intentionally selected to be before and after the first torque drop, respectively. The angles of 66° and 80° are before and after the second torque drop. Both energy and morphology changes suggest that the first step corresponds to the onset of buckling of individual tubes, which is featured by inward deformation and flattening of tubes. After this step, a steady-state period begins in which the partially buckled CNTs require no additional force to buckle further. The second torque drop is caused by the partial detachments of neighboring tubes, under severe buckling and deformation. The arrow in Fig. 2(b), at 66°, points to a position where a large separation between two CNTs occurs at larger torsional angles. The separation is visible in Fig. 2(a), with empty space appearing in the middle of the bundle at 66°. For much larger bundles, the separation is difficult due to the confinements from other tubes. This explains why there are no second torque drops in large bundles (19 CNT).

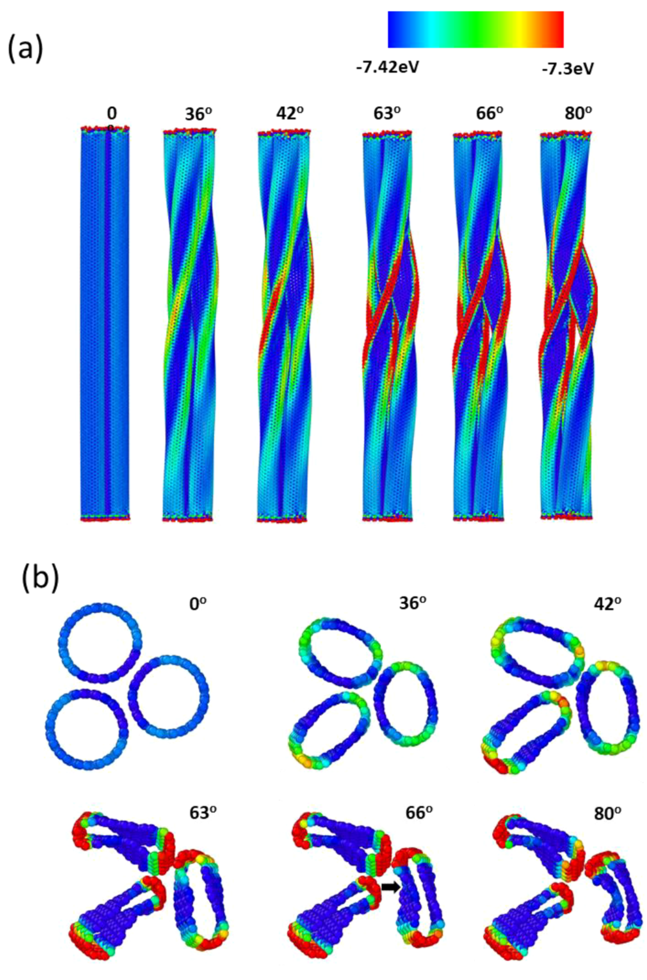

FIG. 2. (a) The side views and (b) the cross-sectional views of the pristine 3 CNT bundle at different torsional angles.

For the irradiated bundles, Figs. 1(a)–1(d) show that radiation damage can significantly change CNT buckling behaviors for 3 CNT, 7 CNT, and 12 CNT bundles. The effects are noticeable even for the lowest damage level (100 ion bombardments): with increasing damage levels, the amplitudes of the first torque drops (in the two-step buckling) become less, in comparison with the pristine CNTs. Furthermore, the torsional angles corresponding to the secondary torque drops become larger. The secondary torque drop is barely observable for large bundles (12 CNT and 19 CNT bundles), regardless of whether the bundles are irradiated or not. For the 7 CNT bundle, the secondary drops disappear for ion bombardment >200 particles. Figure 1(d) shows that the overall irradiation effects of the largest bundle are weaker in comparison with smaller CNT bundles. As to be discussed, this is due to the size effect such that buckling resistance is increased in a very large bundle due to enhanced tube–tube interactions under loading, even without ion irradiation.

Figures 3(a)–3(c) quantitatively compare the buckling behaviors of bundles with or without irradiation damage. For both 3 CNT and 7 CNT bundles, the critical buckling torque and torsional stiffness decrease, whereas the critical buckling angle is increasing with increasing irradiation damage. However, the weakening effects in 7 CNT bundles are not as prominent as they are in the 3 CNT bundle. In contrast to the 3 and 7 CNT bundles, the 12 CNT bundle shows an increase in all three properties. The critical buckling torque is seen to increase by ∼50% at the highest irradiation dose. Likewise, the critical buckling angle is seen to increase from 43° to 77° and the stiffness increases by ∼7%. At 600 ion bombardment, the irradiation enhancement has still not saturated, which indicates the CNT bundle's ability to retain its torsional strength at high concentrations of intra-tube defects. Thus, the critical buckling torque and critical buckling angle can be substantially altered by irradiation of CNT bundles, decreasing for bundles smaller than 7 CNTs and increasing for larger bundles.

To understand the torsional response of irradiated CNT bundles, we compared the atomic scale details of the torsional process in different bundle sizes. Figures 4(a) and 4(b) show cross-sectional views of the 3 CNT bundle and 12 CNT bundle (pristine vs 600-ion-irradiated) at torsional angles of 0°, 54°, and 74°. For both bundles, the irradiation leads to visible inter- and intra-tube defects. Both bundles show strong inter-tube cross-linking occurring. As torque is applied to the system, the CNTs in the pristine CNT bundle are seen to easily rearrange, whereas the irradiated bundle sees little rearrangement. This deformation resistance observed in the irradiated bundle is due to the presence of inter-tube cross-linking defects. By 74°, all the CNTs in the pristine bundle have buckled. In contrast, only a couple of the outer CNTs in the irradiated bundle have buckled. In irradiated bundles, inter-tube defects act as anchoring points which fix the walls of neighboring CNTs together. Thus, the inter-tube defects prevent the CNT walls from buckling inward ultimately leading to an increase in critical buckling strength and critical buckling angle. Figure 4 also explains why the irradiation effects are most prominent in large bundles. For 3 CNT bundles, the amount of "touching" is less than 12 CNT bundles due to its large surface to volume ratios.

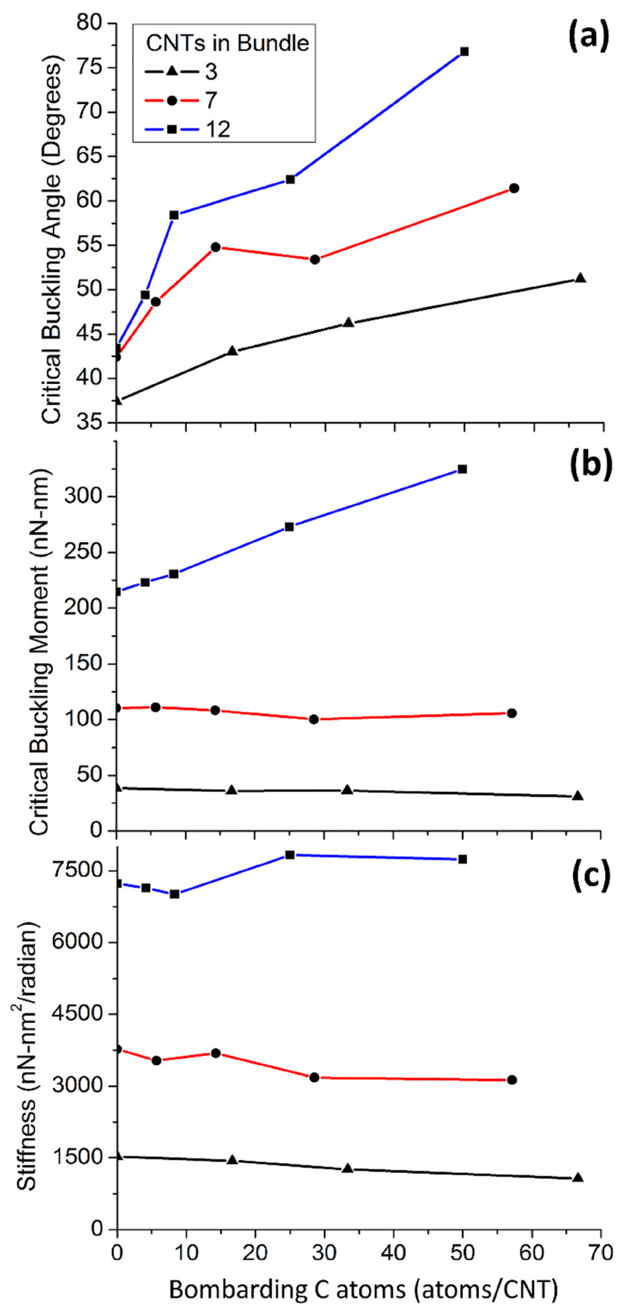

FIG. 3. (a) Critical buckling angle, (b) critical buckling torque, and (c) torsional stiffness for bundles of 3, 7, and 12 CNTs, as a function of the number of bombarding C atoms.

The drop in critical buckling torque for smaller bundles can be understood from Fig. 4 as well. The buckling resistance of individual CNTs in a bundle is largely influence by the number of nearest neighboring CNTs or equivalently the coordination number of the CNT. Highly coordinated CNTs will tend to form inter-tube bonds in multiple directions. For the 3 CNT bundle, each CNT is surrounded by two other CNTs, leaving the majority of sides open to buckling. In the 7 CNT bundle, the central CNT is surrounded by six CNTs and the others are surrounded by three each. This means the central CNT is likely to experience an increased buckling resistance. However, the outer CNTs are able to buckle, since they are only anchored in three of the six possible directions. In the 12 CNT bundle, 3 CNTs are sixfold coordinated 3 are fourfold coordinated and the remaining 6 are threefold coordinated. The lack of sufficient multidirectional anchoring in the 3 and 7 CNT bundles leads to a decrease in critical buckling load for these systems.

As shown in Fig. 1(d), the irradiation enhancement effects are less obvious for the 19 CNT bundle. It is due to the reason that the unirradiated large bundle has a higher buckling resistance than smaller bundles. Note that when two CNT bundles deform and touch each other, the interactions help increase the buckling resistance. Such effects are dominant in large bundles, due to the high coordination number of inside bundles and increased numbers of inside bundles. Furthermore, due to longer moving lengths required for the outside CNTs under torsional loading, these outside CNTs apply higher stress on inside CNTs (in an amplitude more than the outside CNTs of smaller bundles), confine inside ones, and increase the interactions of insider tubes.

In addition to providing multidirectional anchoring, the highly coordinated CNTs have a greater number of possible sites to create inter-tube bonds. Inter-tube defects refer to interstitial atoms, which have interactions between two tubes. As the first step, C displacements stop on the outside surface of a CNT as interstitials. Then they become inter-tube defects when two CNTs are close enough to allow defects to induce interactions with atoms on both tube surfaces through sp, sp^2, or sp^3 bond formation. If such interactions cannot be established, they become intra-tube defects. Therefore, intra-defects include vacancies on the tube, interstitials on the inner surface of a tube, and interstitials on the outside surface without interactions with other tubes. The formation of intra-tube defects is determined by ion–solid interactions, including bombarding species, bombardment energy, and bundle configurations. In the present study, radiation damage creation is random but homogenous since the projected range of carbon atoms is larger than the bundle radius. The formation of inter-tube defects, however, is sensitive to bundle configurations, requiring close touching of neighboring CNTs. For inter-tube defects, forming linkages across larger distances requires multiple atoms in a chain which is less likely to occur. Thus, the number of inter-tube bonds is related to the coordination number of a CNT. The dependence of buckling resistance on CNT coordination number can be seen in the irradiated case of Fig. 4, in which the lower coordinated CNTs start buckling while the inner CNTs deform to pull against the inter-tube bonds but have not started to buckle yet. As the simulation continues, CNTs are seen to buckle starting at lower coordinated CNTs and eventually moving to the highly coordinated CNTs. Thus, the increase in critical buckling torque and critical buckling angle is due to inter-tube bonds anchoring the CNT walls together and thus preventing the inward buckling, which tends to create large separations between neighboring CNTs.

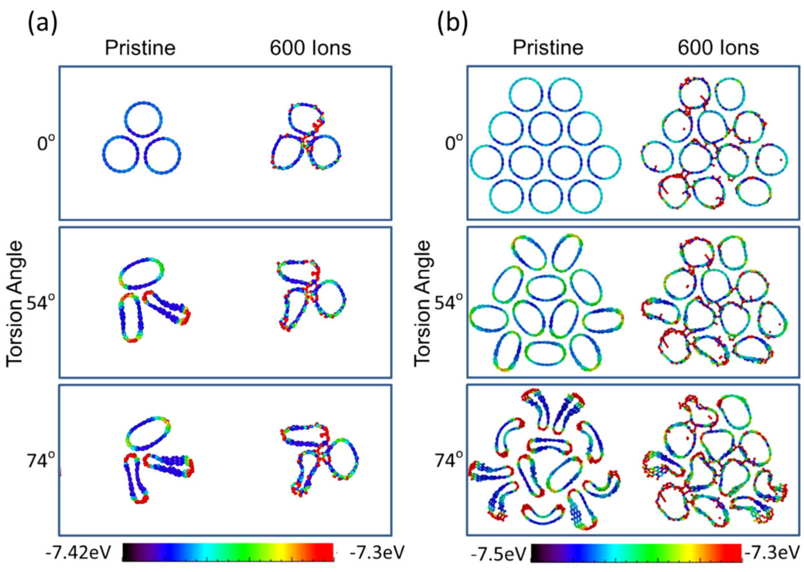

FIG. 4. Cross-sectional views of (a) 3 CNT bundle (left: pristine; right: irradiated by 600 C ions) and (b) 12 CNT bundle (left: pristine; right: irradiated by 600 ions) at torsional angles of 0°, 54°, and 74°. The color refers to potential energy.

The stiffness increase in larger CNT bundles is also due to the creation of inter-tube bonds. However, the mechanism by which the inter-tube bonding increases the stiffness is different. Zhang *et al.* showed using molecular dynamics that the torsional stiffness decreased upon introducing vacancies into the system due to weakening of the CNT wall.[13] This can explain the drop in stiffness observed for the 3 and 7 CNT bundles but does not explain why the stiffness should increase in the 12 CNT bundle. To understand

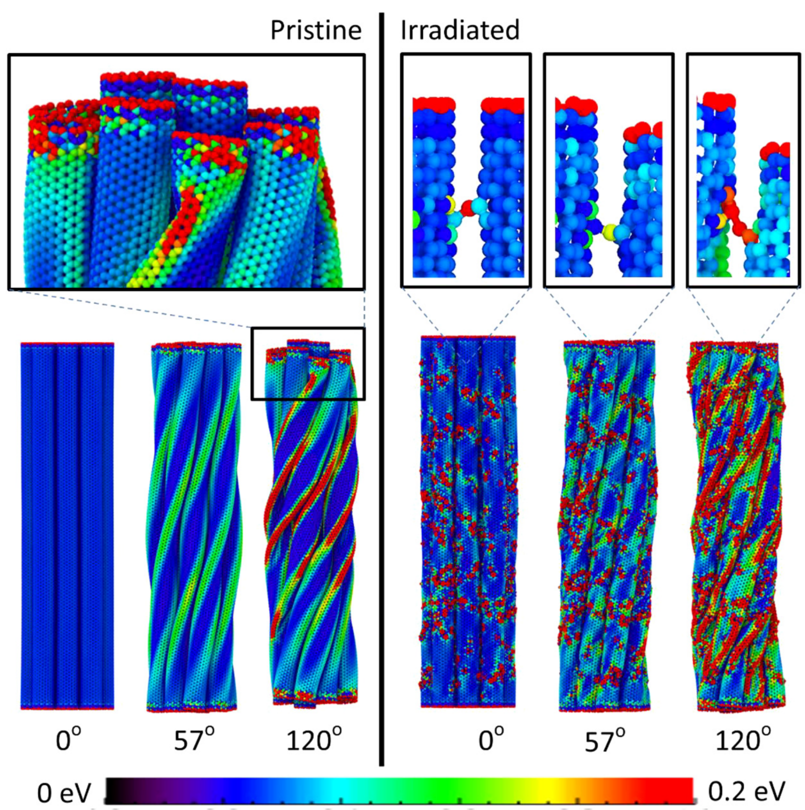

FIG. 5. Pristine and 600 ion-irradiated 12 CNT bundle at given torsional angles with atoms color coded according to potential energy. The pristine bundle shows slip between inner and outer CNTs while the irradiated bundle shows very little slip due to sliding resistance from inter-tube defects.

this phenomenon, we look at the pristine 12 CNT bundle at various torsional angles (Fig. 5). As the torsional angle is increased, the CNTs in the outer layers begin to slip relative to the inner CNTs as shown in the inset in Fig. 5. This slip is due to the fact that the outer CNTs must follow a longer path around than the inner CNTs. The distance that a CNT must follow is given to a rough approximation by arc length of a helix,

$$s = \sqrt{(r\theta)^2 + L^2}. \tag{1}$$

Using Eq. (1), we find that the difference in arc length between the innermost and outermost CNTs in the 3, 7, and 12 CNT bundle is 0 Å, 2.5 Å, and 5.2 Å respectively. In the pristine bundle, the tubes can easily slip relative to one another. In contrast, the irradiated bundle has multiple inter-tube bonds that prevent the CNTs from slipping and by consequence introduces a tensile strain into the system. This effect can most easily be seen at the ends of the bundle where the slip is greatest. Figure 5 shows the time evolution of an inter-tube bond between an inner and outer CNT as torsion is applied to the system. As the slip increases, the inter-tube bond begins to pull out a chain of atoms and the angle between the CNTs and bond decreases. Until the angle between the bond and the CNTs decreases appreciably, the inter-tube bond will not be able to provide much resistance to slip. In the 3 CNT bundle, all tubes are at the same relative distance from the torsional axis and as a result will not experience slip. Thus, the irradiated 3 CNT bundle sees a decrease in stiffness due to CNT wall weakening from intra-tube defects. The 7 CNT shows a slightly smaller decrease in torsional stiffness. Very little slip is observed in either the pristine 3 or 7 CNT bundles leading to the conclusion that the difference in path length between the tubes is too small to reorient the inter-tube bonds and have an effect on the stiffness. Equation (1) also implies that the stiffness will depend on the length of the bundle. This formula can be rewritten to keep a constant torsional angle per unit length by defining $\theta^*=\theta/L$. Using this θ^*, Eq. (1) can be rewritten as

$$s = L\sqrt{(r\theta^*)^2 + 1}. \tag{2}$$

Thus, the difference in path length between inner and outer CNTs will increase linearly with increasing length of the bundle given a constant torsional angle per unit length θ^*. For larger slip between CNTs, more inter-tube bonds will be reoriented to resist the sliding motion and thus the stiffness will increase. From Fig. 5 and the above discussion, we arrive at the conclusion that the increase in stiffness is due to the resistance to CNT slip provided by the inter-tube bonding. In addition, the stiffness will be greater for longer bundles given the same irradiation density due to the increased path length difference between outer and inner CNTs.

Figure 5 clearly shows that upon slipping, inter-tube defects act as seeds to induce the formation of short single carbon atomic chains (SCACs). Such SCAC formation has been suggested previously from both experimental and modeling studies on other low dimensional carbon systems.[29–37] Individual SCACs have been observed before in gas-phase deposition, epitaxial growth, electrochemical synthesis, and thinning of carbon nanoribbons.[30–37] Various modeling studies suggested that SCAC is a metastable configuration.[38–40] In one of our recent study, it was observed that inter-plane interstitials trapping between graphene planes can induce SCACs upon graphene sliding. The seed atoms pull carbon atoms one by one from the graphene and can form a long SCAC to affect the frictional resistance.[41]

The present study shows the feasibility of using ion irradiation to improve buckling resistance of CNT bundles. As shown by many previous studies on a wide range of materials not limited to CNTs, localized structural modification, or precisely engineered imperfections, can significantly improve bucking resistance of metamaterials and structural components.[42–44] By introducing "imperfection by design," many studies have demonstrated deterministic and programmable material behaviors.[42–51] It is feasible to trigger a controllable and predictable buckling, leading to unique "energy trapping" and enhanced loading capability.[50] Controllable bucking can also be used as building blocks to obtain unique bulk mechanical properties.[51]

IV. CONCLUSION

In this study, we have shown that irradiation damage can have a profound effect on the torsional properties of CNT bundles. The effect, however, is size dependent. Bundles smaller than the 12 CNT bundle show a slight decrease in torsional stiffness and an increase in the critical buckling angle. In contrast, 12 CNT bundles show an increase in the critical buckling torque and critical buckling angle and a slight increase in torsional stiffness. All changes can be linked to the creation of intra-tube and inter-tube defects. The intra-tube defects tend to lower the critical buckling torque and torsional stiffness while the inter-tube defects are seen to increase the critical buckling torque, critical buckling angle, and torsional stiffness for the larger CNT bundles. The increase in critical buckling load observed in the large bundles is due to inter-tube bonds keeping the walls of CNTs anchored together and thus preventing buckling. The increase in stiffness is also due to the inter-tube bonding increasing the sheer modulus for slip between neighboring CNTs. As the CNT bundle is torqued, the inter-tube bonds at the bundle ends begin to stretch and pull out a chain of atoms. The irradiation-induced stiffening is predicted to have a more profound effect in longer bundles. This effect is the result of the difference in path lengths between the innermost and outermost CNTs when under a torsional load. The above size effects become weak for the largest 19 CNT bundle due to the fact the inter-tube interactions are already promoted in a very large bundle even without ion irradiation. The studies will impact the technological development of using ion beam modification to induce cross-linking in CNT bundles to improve overall strength. The findings will benefit the design of future nanoelectromechanical systems, nanoactuators, and nanocomposites.

ACKNOWLEDGMENTS

This work was supported by the U.S. Department of Energy, Office of Basic Energy Sciences, under Grant No. DE-SC0006725.

DATA AVAILABILITY

The data that support the findings of this study are available from the corresponding author upon reasonable request.

REFERENCES

[1]A. V. Krasheninnikov and F. Banhart, "Engineering of nanostructured carbon materials with electron or ion beams," Nat. Mater. **6**(10), 723–733 (2007).
[2]A. Kis, G. Csányi, J.-P. Salvetat *et al.*, "Reinforcement of single-walled carbon nanotube bundles by intertube bridging," Nat. Mater. **3**(3), 153–157 (2004).
[3]J. G. Gigax, P. D. Bradford, and L. Shao, "Ion beam modification of carbon nanotube yarn in air and vacuum," Materials **10**(8), 860 (2017).
[4]T. Filleter, R. Bernal, S. Li *et al.*, "Ultrahigh strength and stiffness in cross-linked hierarchical carbon nanotube bundles," Adv. Mater. **23**(25), 2855–2860 (2011).
[5]M. Sammalkorpi, A. V. Krasheninnikov, A. Kuronen, K. Nordlund, and K. Kaski, "Irradiation-induced stiffening of carbon nanotube bundles," Nucl. Instrum. Methods Phys. Res. Sect. B **228**(1), 142–145 (2005).
[6]M. Dequesnes, S. V. Rotkin, and N. R. Aluru, "Calculation of pull-in voltages for carbon-nanotube-based nanoelectromechanical switches," Nanotechnology **13**(1), 120–131 (2002).
[7]A. M. Fennimore, T. D. Yuzvinsky, Wei-Qiang Han, M. S. Fuhrer, J. Cumings, and A. Zettl, "Rotational actuators based on carbon nanotubes," Nature **424**, 408–410 (2003).
[8]S. J. Papadakis, A. R. Hall, P. A. Williams *et al.*, "Resonant oscillators with carbon-nanotube torsion springs," Phys. Rev. Lett. **93**(14), 146101 (2004).
[9]J. Cumings, "Low-friction nanoscale linear bearing realized from multiwall carbon nanotubes," Science **289**(5479), 602–604 (2000).
[10]M. J. Biercuk, M. C. Llaguno, M. Radosavljevic *et al.*, "Carbon nanotube composites for thermal management," Appl. Phys. Lett. **80**(15), 2767–2769 (2002).
[11]O. Breuer and U. Sundararaj, "Big returns from small fibers: A review of polymer/carbon nanotube composites," Polym. Compos. **25**(6), 630–645 (2004).
[12]B. I. Yakobson, C. J. Brabec, and J. Bernholc, "Nanomechanics of carbon tubes: Instabilities beyond linear response," Phys. Rev. Lett. **76**(14), 2511–2514 (1996).
[13]Y. Y. Zhang, C. M. Wang, and Y. Xiang, "A molecular dynamics investigation of the torsional responses of defective single-walled carbon nanotubes," Carbon **48**(14), 4100–4108 (2010).
[14]V. Vijayaraghavan and C. H. Wong, "Temperature, defect and size effect on the elastic properties of imperfectly straight carbon nanotubes by using molecular dynamics simulation," Comput. Mater. Sci. **71**, 184–191 (2013).
[15]A. Fereidoon, M. Ghorbanzadeh Ahangari, M. D. Ganji, and M. Jahanshahi, "Density functional theory investigation of the mechanical properties of single-walled carbon nanotubes," Comput. Mater. Sci. **53**, 377–381 (2012).
[16]B.-W. Jeong and H.-Y. Kim, "Molecular dynamics simulations of the failure behaviors of closed carbon nanotubes fully filled with C60 fullerenes," Comput. Mater. Sci. **77**, 7–12 (2013).
[17]V. Vijayaraghavan and C. H. Wong, "Nanomechanics of single walled carbon nanotube with water interactions under axial tension by using molecular dynamics simulations," Comput. Mater. Sci. **79**, 519–526 (2013).
[18]Y. Y. Zhang, C. M. Wang, and Y. Xiang, "Bending behavior of double-walled carbon nanotube with sp^3 interwall bonds," J. Appl. Phys. **109**, 083516 (2011).
[19]P. R. Guduru and Z. Xia, "Shell buckling of imperfect multiwalled carbon nanotubes—Experiments and analysis," Exp. Mech. **47**, 153 (2007).
[20]Z. H. Xia, P. R. Guduru, and W. A. Curtin, "Enhancing mechanical properties of multiwall carbon nanotubes via sp^3 interwall bridging," Phys. Rev. Lett. **98**, 245501 (2007).
[21]G. A. Shen, S. Namilae, and N. Chandra, Mater. Sci. Eng. A **429**, 66 (2006).
[22]B. Peng, M. Locascio, P. Zapol, S. Li, S. L. Mielke, G. C. Schatz, and H. D. Espinosa, "Measurements of near-ultimate strength for multiwalled carbon nanotubes and irradiation-induced crosslinking improvement," Nat. Nanotechnol. **3**, 626–631 (2008).
[23]S. Plimpton, "Fast parallel algorithms for short-range molecular dynamics," J. Comput. Phys. **117**, 1–19 (1995).
[24]G. E. Bacon, "The interlayer spacing of graphite," Acta Crystallogr. **4**(6), 558–561 (1951).
[25]J. Tersoff, "Modeling solid-state chemistry: Interatomic potentials for multicomponent systems," Phys. Rev. B **39**(8), 5566–5568 (1989).
[26]J. F. Ziegler, J. P. Biersack, and U. Littmark, *Stopping and Ranges of Ions in Matter* (Pergamon Press, 1985).
[27]T. Schneider and E. Stoll, "Molecular-dynamics study of a three-dimensional one-component model for distortive phase transitions," Phys. Rev. B **17**(3), 1302–1322 (1978).
[28]S. J. Stuart, A. B. Tutein, and J. A. Harrison, "A reactive potential for hydrocarbons with intermolecular interactions," J. Chem. Phys. **112**(14), 6472–6486 (2000).
[29]A. E. Goresy and G. Donnay, "A new allotropic form of carbon from the Ries crater," Science **161**, 363–364 (1968).
[30]R. J. Lagow, J. J. Kampa, H.-C. Wei *et al.*, "Synthesis of linear acetylenic carbon: The "sp" carbon allotrope," Science **267**, 362–367 (1995).
[31]L. Kavan, J. Hlavatý, J. Kastner, and H. Kuzmany, "Electrochemical carbyne from perfluorinated hydrocarbons: Synthesis and stability studied by Raman scattering," Carbon **33**, 1321–1329 (1995).
[32]C. S. Casari, A. L. Bassi, L. Ravagnan *et al.*, "Chemical and thermal stability of carbyne-like structures in cluster-assembled carbon films," Phys. Rev. B **69**, 075422 (2004).
[33]F. Cataldo, *Polyynes: Synthesis, Properties, and Applications* (CRC Press, 2005).
[34]C. Jin, H. Lan, L. Peng, K. Suenaga, and S. Iijima, "Deriving carbon atomic chains from graphene," Phys. Rev. Lett. **102**, 205501 (2009).
[35]E. Hobi, R. B. Pontes, A. Fazzio, and A. J. R. da Silva, "Formation of atomic carbon chains from graphene nanoribbons," Phys. Rev. B **81**, 201406 (2010).
[36]A. Chuvilin, J. C. Meyer, G. Algara-Siller, and U. Kaiser, "From graphene constrictions to single carbon chains," New J. Phys. **11**, 083019 (2009).
[37]F. Börrnert, C. Börrnert, S. Gorantla *et al.*, "Single-wall-carbon-nanotube/single-carbon-chain molecular junctions," Phys. Rev. B **81**, 085439 (2010).
[38]I. E. Castelli, N. Ferri, G. Onida, and N. Manini, "Carbon sp chains in graphene nanoholes," J. Phys. Condens. Matter **24**, 104019 (2012).
[39]C. Ataca and S. Ciraci, "Perpendicular growth of carbon chains on graphene from first-principles," Phys. Rev. B **83**, 235417 (2011).
[40]Y. Wang, Z.-Z. Lin, W. Zhang, J. Zhuang, and X.-J. Ning, "Pulling long linear atomic chains from graphene: Molecular dynamics simulations," Phys. Rev. B **80**, 233403 (2009).
[41]J. B. Wallace, D. Chen, and L. Shao, "Carbon displacement induced single carbon atomic chain formation and its effects on sliding of SiC fibers in SiC/graphene/SiC composite," Mater. Res. Lett. **4**(1), 55–61 (2016).
[42]J. Paulose, A. S. Meeussen, and V. Vitelli, "Selective buckling via states of self-stress in topological metamaterials," Proc. Natl. Acad. Sci. U.S.A. **112**, 7639–7644 (2015).
[43]A. Lee, F. López Jiménez, J. Marthelot, J. W. Hutchinson, and P. M. Reis, "The geometric role of precisely engineered imperfections on the critical buckling load of spherical elastic shells," J. Appl. Mech. **83**, 111005–111011 (2016).
[44]N. Hu and R. Burgueño, "Tailoring the elastic postbuckling response of cylindrical shells: A route for exploiting instabilities in materials and mechanical systems," Extreme Mech. Lett. **4**, 103–110 (2015).
[45]Y. Tang, G. Lin, S. Yang, Y. K. Yi, R. D. Kamien, and J. Yin, Adv. Mater. **29**, 1604262 (2017).
[46]B. S. Cox, R. M. J. Groh, and A. Pirrera, "Nudging axially compressed cylindrical panels toward imperfection insensitivity," J. Appl. Mech. **86**, 071010 (2019).
[47]B. S. Cox, R. M. J. Groh, D. Avitabile, and A. Pirrera, "Modal nudging in nonlinear elasticity: Tailoring the elastic post-buckling behaviour of engineering structures," J. Mech. Phys. Solids **116**, 135–149 (2018).
[48]Y. Yang, M. A. Dias, and D. P. Holmes, "Multistable kirigami for tunable architected materials," Phys. Rev. Mater. **2**, 110601 (2018).

[49]C. Mo and J. R. Raney, "Spatial programming of defect distributions to enhance material failure characteristics," Extreme Mech. Lett. **34**, 100598 (2020).
[50]Y. Zhao, A. J. J. Maria Joseph, Z. Zhang, C. Ma, D. Gul, A. Schellenberg, and N. Hu, "Deterministic snap-through buckling and energy trapping in axially-loaded notched strips for compliant building blocks," Smart Mater. Struct. **29**, 02LT03 (2020).
[51]C. Coulais, A. Sabbadini, F. Vink, and M. van Hecke, "Multi-step self-guided pathways for shape-changing metamaterials," Nature **561**, 512–515 (2018).